A&A 554, A49 (2013)
DOI: 10.1051/0004-6361/201219859

Astronomy & Astrophysics

Photometry and taxonomy of trans-Neptunian objects and Centaurs in support of a *Herschel* key program⋆

D. Perna[1], E. Dotto[2], M. A. Barucci[1], E. Mazzotta Epifani[3], E. Vilenius[4], M. Dall'Ora[3], S. Fornasier[1,5], and T. G. Müller[4]

[1] LESIA – Observatoire de Paris, CNRS, UPMC Univ. Paris 06, Univ. Paris-Diderot, 5 place J. Janssen, 92195 Meudon, France
e-mail: davide.perna@obspm.fr
[2] INAF – Osservatorio Astronomico di Roma, Via Frascati 33, 00040 Monte Porzio Catone (Roma), Italy
[3] INAF – Osservatorio Astronomico di Capodimonte, Salita Moiariello 16, 80131 Napoli, Italy
[4] Max–Planck–Institut für extraterrestrische Physik, Postfach 1312, Giessenbachstr., 85741 Garching, Germany
[5] Univ. Paris Diderot, Sorbonne Paris Cité, 4 rue Elsa Morante, 75205 Paris, France

Received 21 June 2012 / Accepted 12 April 2013

ABSTRACT

Context. The investigation of Centaurs and trans-Neptunian objects (TNOs) provides essential information about the early conditions and evolution of the outer solar system. The radiometric technique combines measurements in the visible and thermal infrared; with these one can estimate the size and albedo of Centaurs and TNOs.
Aims. Our aim is to obtain visible photometry of a sample of Centaurs and TNOs, a subset of the targets of the "TNOs are cool" key program at the *Herschel* Space Observatory.
Methods. We carried out visible photometry of Centaurs and TNOs, making use of the DOLORES instrument at the Telescopio Nazionale *Galileo* (TNG, La Palma, Spain).
Results. We report photometric observations of 20 objects and present the computed absolute magnitudes. We derive the taxonomy of our targets (nine are classified for the first time, the results for five objects agree with the literature, the other targets are tentatively classified based on incomplete datasets) and combine the results with the literature, searching for correlations between taxonomy and dynamics. We look for comet-like activity in our Centaur sample, including (248835) 2006 SX368, which was previously described as active.
Conclusions. We provide an accurate determination of the absolute magnitude and of the relative error for each of our targets. These values can be readily used in combination with thermal infrared data. The surface of TNO (65489) Ceto seems to be heterogeneous. Our results seem to support an evolutionary origin for the color dichotomy of Centaurs, and the occurrence of a strong mixing after the TNO formation. No evident cometary activity is detected around the five Centaurs in our sample; assuming that an unresolved coma is present around (248835) 2006 SX368, we use the "photometric model" to derive the possible dust production rate, finding that $Q_{\rm dust}$ is in the range 1–31 kg/s.

Key words. Kuiper belt: general – techniques: photometric

1. Introduction

Trans-Neptunian objects (TNOs) and Centaurs represent the remnants of the leftover planetesimals from the early accretional phases of the outer pre-planetary disk, hence the study of the physical properties of these objects is fundamental to constrain the formation and evolution of the outer solar system (e.g., Barucci et al. 2008). In particular, the radiometric technique combines information from the thermal infrared emission and the visible magnitude to derive the albedo and the diameter of these distant and icy bodies (e.g., Stansberry et al. 2008). The "TNOs are cool" key program (Müller et al. 2009) at the *Herschel* Space Observatory significantly contributes to our understanding of TNO science; it observes ∼130 objects with typical diameters ≳150 km in the thermal infrared. These large bodies are assumed to be almost unchanged from the accretion phases (Davis & Farinella 1997), hence the currently obtained size distribution reflects the primordial distribution of the outer planetesimals. More information on the early evolution of the solar system can be retrieved from possible correlations between the size, the albedo, and other physical and orbital parameters of the targets.

In support of the "TNOs are cool" program, we performed visible photometry of 20 TNOs and Centaurs, selected among the targets of the program at the *Herschel* Space Observatory. In this paper we derive the absolute magnitude H_V of the targets, information fundamental for interpreting the *Herschel* data. Moreover, the $B-V$, $V-R$, $V-I$ colors give us a first indication about the targets' surface composition. We therefore combine our results with the available literature, looking for correlations between colors and dynamical properties of TNOs and Centaurs. Finally, we search for cometary activity around the five Centaurs in our sample, and in particular for (248835) 2006 SX368, which was previously reported as active (Jewitt 2009).

⋆ Based on observations made with the Italian Telescopio Nazionale *Galileo* (TNG) operated on the island of La Palma by the Fundacion Galileo Galilei of the INAF (Istituto Nazionale di Astrofisica) at the Spanish Observatorio del Roque de los Muchachos of the Instituto de Astrofisica de Canarias (programs AOT19/TAC33, AOT20/TAC45, and AOT21/TAC56).

2. Observations and data reduction

Observations were carried out at the 3.58 m Telescopio Nazionale *Galileo* (TNG, La Palma, Spain) during three runs (June 2009, October 2009, June 2010) for a total of ten observing nights. Visible photometry was performed with the DOLORES (Device Optimized for the LOw RESolution) instrument, equipped with a 2048 × 2048 E2V 4240 thinned back-illuminated, deep-depleted, Astro-*BB* coated CCD with a pixel size of 13.5 μm. The field of view is 8.6 × 8.6 arcmin, with a 0.252 arcsec/pixel scale. We used the broadband B, V, R, I filters, adjusting the exposure time according to the object magnitude and sky conditions. Typically, we used a *VBRIV* photometric sequence, repeating the V filter twice to check for color variations caused by rotational light curves. Each sequence lasted for about 40–90 min, depending on the object brightness and the filters actually used. The observational circumstances are given in Table 1, which also lists the dynamical classification of the objects (according to the system by Gladman et al. 2008).

The images were reduced using standard procedures with the MIDAS software package: after subtraction of the bias from the raw data and flat-field correction (for each filter we used the median of several twilight exposures), the instrumental magnitudes were measured via aperture photometry, with an integrating radius typically about three times the average seeing and sky subtraction performed using a 5–10-pixel-wide annulus around each object. The aperture correction method (e.g., Barucci et al. 2000) was used for only a few cases (faint target and/or nearby field stars) to determine the object flux. The absolute calibration of the magnitudes was obtained by means of the observation of several Landolt (1992) standard fields.

3. Results and analysis

Table 2 lists the derived magnitudes of the 20 observed objects. For each *VBRIV* photometric sequence we report the two obtained V magnitudes and the mean $B-V$, $V-R$, $V-I$ colors. Missing values (long dash) indicate that the sequence was not completed (because of the faintness of the target – especially for the B filter –, changed observability conditions, etc.) or that the obtained photometric values were judged to be unreliable (because of poor signal-to-noise ratio, cosmic rays, etc.).

For each target, the different measurements agree well with each other: the observed weak variations in the V magnitudes are easily explained by geometry (changing heliocentric and topocentric distances, see Table 1) or light curve variability (whenever available in the literature, we also report the light curve amplitude in Table 2), and the reported colors are consistent with the literature whenever available. The only relevant exception concerns the $V-I$ color of (65489) Ceto, which presents a considerable variation, up to ∼0.5 mag. Grundy et al. (2007) have found this object to be a binary system (Ceto/Phorcys), for which they reported an average $V-I$ color of 1.07 ± 0.04 mag, without statistically significant differences between the two components. Most of our measurements are consistent or only slightly discrepant with this value, while the difference with the $V-I$ color obtained on June 12, 2010 (0.63 ± 0.08 mag) is clearly beyond the statistical uncertainty. This could suggest possible surface heterogeneity (Dotto et al. 2008, reported a double peaked rotational light curve of period 4.43 ± 0.03 h and amplitude 0.13 ± 0.02 mag for this object). The $B-V$ and $V-R$ colors that we report for (65489) Ceto instead agree with the literature.

3.1. Absolute magnitudes

As stated above, the absolute magnitude H_V of an object can be used, in combination with thermal data, to derive its diameter and albedo through the radiometric technique. Once determinations of the albedo and size are available for the whole ∼130 TNOs and Centaurs that are targets of the *Herschel* program, fundamental information on the formation and early evolution of the solar system can be obtained through studying the (∼primordial) size distribution and the possible correlations between the albedo, size, color/spectra, and orbital parameters of the objects.

We stress how important an accurate determination of H_V is when applying the radiometric technique. Indeed, while errors on the absolute magnitude have limited influence on the determined radiometric size, they do play a key role for the albedo (see, e.g., Vilenius et al. 2012): an error of ±0.1 mag on H_V influences the geometric albedo by about ±10%; a ±0.3 mag error would produce a ±30% relative error in geometric albedo. Hence we were very careful when we determined H_V and its error for each of our targets, to provide "ready-to-use" values for modelers using the radiometric technique.

The equation used to calculate the absolute magnitude is

$$H_V = V - 5\log(r\Delta) - \alpha\beta - 0.1 = H(\alpha) - \alpha\beta - 0.1, \quad (1)$$

where V represents the visible magnitude, Δ, r and α are the topocentric and heliocentric distances and the phase angle given in Table 1, respectively, and β is the phase curve slope (mag/deg). The magnitudes $H(\alpha)$ reduced at $\Delta = r = 1$ are listed in Table 2. As for the phase effect, we recall that the phase curve behavior near opposition for TNOs and Centaurs is nonlinear, and that the IAU (H, G) magnitude system (Bowell et al. 1989) is known to describe the photometric phase curves of these objects only poorly (see Belskaya et al. 2008, for a review on the phase curve behavior of TNOs and Centaurs). Literature data indicate that the photometric phase curves of TNOs and Centaurs present a steep linear behavior up to very small phase angles, and that a very narrow opposition surge starts only at $\alpha \lesssim 0.1°$–$0.2°$. All available observations at such very low phase angles indicate an opposition surge of ∼0.1 mag with respect to a linear phase behavior (see Belskaya et al. 2008, and references therein). Because we lack a better system, we hence assumed a linear approximation for the magnitude dependence on the phase angle, then subtracted an a priori quantity of 0.1 mag to derive our final results of H_V, taking into account an unseen opposition surge effect (all of our measurements were performed at phase angles larger than 0.4°).

To compute the phase curve slope β, we firstly checked the literature for reliable data to be combined with our measurements. We stress that, given the very limited range of phase angles spanned by the observations of TNOs and Centaurs, including photometric points of poor quality (i.e., errors $\gtrsim$0.05 mag), and/or acquired at nearly the same phase angle (i.e., phase angle range $\lesssim$0.5°) in our analysis, could lead to very unsatisfactory results. Hence, we used different approaches for our targets: if at least two good-quality measuremnts of $H(\alpha)$ were available at well-separated phase angles, we performed a fit of the available data and found β and H_V. This is the case of Ceto, 2003 CO1, 2003 OP32, Salacia, 2005 RN43, and 2008 FC76. For all other objects (when all available photometric points lie at the same or very similar α, or several points are of poor photometric quality) we assumed an a priori value of $\beta = 0.12 \pm 0.06$ mag/deg for TNOs, and $\beta = 0.09 \pm 0.04$ mag/deg for Centaurs (for these cases, we propagated the maximum error of the assumed slope on the

Table 1. Observational circumstances.

Object	Dyn. class	Date	UT_{start}	Δ (AU)	r (AU)	α (deg)
(65489) Ceto [2003 FX128]	scattered	22 Jun. 2009	22:39	30.091	30.623	1.6
		23 Jun. 2009	21:53	30.107	30.625	1.6
		23 Jun. 2009	23:31	30.108	30.625	1.7
		11 Jun. 2010	01:13	30.788	31.498	1.3
		12 Jun. 2010	01:25	30.802	31.500	1.4
(120061) 2003 CO1	centaur	13 Jun. 2010	00:56	11.029	11.950	2.1
		14 Jun. 2010	01:06	11.038	11.952	2.2
(120178) 2003 OP32	classical	11 Jun. 2010	02:31	41.202	41.533	1.3
		11 Jun. 2010	04:14	41.201	41.533	1.3
		12 Jun. 2010	02:59	41.186	41.533	1.3
(120216) 2004 EW95	resonant (3:2)	10 Jun. 2010	22:12	26.871	27.478	1.7
		11 Jun. 2010	22:30	26.884	27.478	1.7
(120347) Salacia [2004 SB60]	classical	23 Jun. 2009	03:05	43.887	44.059	1.3
		24 Jun. 2009	03:23	43.872	44.059	1.3
		26 Jun. 2009	02:36	43.842	44.060	1.3
(133067) 2003 FB128	resonant (3:2)	12 Jun. 2010	21:45	33.049	33.842	1.1
		13 Jun. 2010	21:45	33.061	33.842	1.1
(136204) 2003 WL7	centaur	15 Oct. 2009	00:38	14.296	15.002	2.8
		15 Oct. 2009	03:14	14.295	15.002	2.8
		16 Oct. 2009	04:01	14.283	15.002	2.7
(145452) 2005 RN43	classical	11 Jun. 2010	03:15	40.407	40.687	1.4
		12 Jun. 2010	03:55	40.391	40.687	1.4
		13 Jun. 2010	02:19	40.376	40.687	1.4
		14 Jun. 2010	03:52	40.359	40.687	1.4
(145480) 2005 TB190	detached	26 Jun. 2009	03:03	46.054	46.401	1.2
(145486) 2005 UJ438	centaur	16 Oct. 2009	02:19	8.136	8.333	6.8
(174567) 2003 MW12	classical	22 Jun. 2009	23:45	46.938	47.823	0.6
		23 Jun. 2009	23:00	46.944	47.823	0.6
		24 Jun. 2009	00:24	46.944	47.823	0.6
(248835) 2006 SX368	centaur	24 Jun. 2009	04:20	11.655	12.013	4.6
		25 Jun. 2009	01:32	11.644	12.013	4.6
		25 Jun. 2009	03:49	11.643	12.013	4.6
(281371) 2008 FC76	centaur	13 Jun. 2010	03:15	10.853	10.947	5.3
		14 Jun. 2010	02:28	10.838	10.946	5.3
(303775) 2005 QU182	scattered	14 Oct. 2009	23:28	47.337	48.282	0.4
		15 Oct. 2009	22:20	47.343	48.283	0.4
		16 Oct. 2009	01:00	47.343	48.284	0.4
(307251) 2002 KW14	classical	25 Jun. 2009	00:20	39.775	40.642	0.8
		25 Jun. 2009	23:33	39.784	40.642	0.8
(307982) 2004 PG115	scattered	23 Jun. 2009	01:36	36.081	36.738	1.2
		23 Jun. 2009	04:16	36.080	36.738	1.2
		24 Jun. 2009	02:11	36.069	36.738	1.2
		14 Oct. 2009	21:46	36.337	36.772	1.4
		15 Oct. 2009	19:43	36.350	36.772	1.4
		15 Oct. 2009	21:17	36.352	36.772	1.4
2003 FE128	resonant (2:1)	24 Jun. 2009	21:53	35.227	35.852	1.3
		25 Jun. 2009	21:49	35.240	35.852	1.3
		12 Jun. 2010	23:04	35.053	35.848	1.0
		13 Jun. 2010	23:32	35.064	35.848	1.0
2003 GH55	classical	10 Jun. 2010	23:29	40.027	40.823	0.9
		12 Jun. 2010	00:05	40.037	40.823	0.9
2004 NT33	classical	23 Jun. 2009	00:59	37.569	38.155	1.3
		23 Jun. 2009	02:25	37.568	38.155	1.3
		24 Jun. 2009	01:34	37.558	38.156	1.2
2007 OC10	detached	25 Jun. 2009	02:37	34.743	35.492	1.1
		26 Jun. 2009	01:19	34.733	35.492	1.1
		26 Jun. 2009	03:49	34.732	35.492	1.1

Notes. Δ, r and α are the topocentric distance, the heliocentric distance, and the phase angle, respectively.

Table 2. Observed magnitudes.

Object	Date	UT_{start}	V	$B-V$	$V-R$	$V-I$	$H(\alpha)$	Light curve ampl.
(65489) Ceto [2003 FX128]	22 Jun. 2009	22:39	21.72 ± 0.03	0.86 ± 0.07	0.52 ± 0.04	1.12 ± 0.06	6.90 ± 0.03	0.13 ± 0.02[a]
			21.72 ± 0.03	...	...	...	6.90 ± 0.03	
	23 Jun. 2009	21:53	21.66 ± 0.05	0.92 ± 0.06	0.54 ± 0.06	0.90 ± 0.08	6.84 ± 0.05	
			21.66 ± 0.04	...	...	...	6.84 ± 0.04	
	23 Jun. 2009	23:31	21.61 ± 0.04	0.95 ± 0.08	0.49 ± 0.07	0.92 ± 0.08	6.79 ± 0.04	
			21.55 ± 0.05	...	...	...	6.73 ± 0.05	
	11 Jun. 2010	01:13	21.83 ± 0.04	–	0.55 ± 0.06	1.20 ± 0.19	6.90 ± 0.04	
	12 Jun. 2010	01:25	21.75 ± 0.06	–	0.59 ± 0.07	0.63 ± 0.08	6.82 ± 0.06	
(120061) 2003 CO1	13 Jun. 2010	00:56	19.97 ± 0.03	0.74 ± 0.04	0.45 ± 0.04	1.02 ± 0.05	9.37 ± 0.03	0.07 ± 0.01[b]
			19.96 ± 0.03	...	...	...	9.36 ± 0.03	
	14 Jun. 2010	01:06	19.92 ± 0.02	0.75 ± 0.05	0.48 ± 0.03	1.01 ± 0.04	9.32 ± 0.02	
			19.91 ± 0.02	...	...	...	9.31 ± 0.02	
(120178) 2003 OP32	11 Jun. 2010	02:31	20.24 ± 0.04	0.65 ± 0.06	0.36 ± 0.05	0.68 ± 0.05	4.07 ± 0.04	0.13 ± 0.01[b]
			20.29 ± 0.04	...	...	...	4.12 ± 0.04	
	11 Jun. 2010	04:14	20.38 ± 0.04	0.67 ± 0.06	0.36 ± 0.06	0.68 ± 0.06	4.21 ± 0.04	
	12 Jun. 2010	02:59	20.28 ± 0.03	0.63 ± 0.05	0.40 ± 0.05	0.63 ± 0.04	4.11 ± 0.03	
			20.31 ± 0.03	...	...	...	4.14 ± 0.03	
(120216) 2004 EW95	10 Jun. 2010	22:12	21.03 ± 0.03	0.67 ± 0.06	0.40 ± 0.05	0.67 ± 0.05	6.69 ± 0.03	not known
			21.02 ± 0.03	...	...	...	6.68 ± 0.03	
	11 Jun. 2010	22:30	21.05 ± 0.04	0.69 ± 0.06	0.36 ± 0.05	0.52 ± 0.05	6.71 ± 0.04	
			21.05 ± 0.04	...	...	...	6.71 ± 0.04	
(120347) Salacia [2004 SB60]	23 Jun. 2009	03:05	20.86 ± 0.03	0.61 ± 0.05	0.42 ± 0.04	0.91 ± 0.07	4.43 ± 0.03	0.03 ± 0.01[b]
			20.86 ± 0.03	...	...	...	4.43 ± 0.03	
	24 Jun. 2009	03:23	20.84 ± 0.05	0.76 ± 0.09	0.40 ± 0.09	0.80 ± 0.15	4.41 ± 0.05	
			20.90 ± 0.06	...	...	...	4.47 ± 0.06	
	26 Jun. 2009	02:36	20.80 ± 0.04	–	0.38 ± 0.06	0.76 ± 0.08	4.37 ± 0.04	
(133067) 2003 FB128	12 Jun. 2010	21:45	22.68 ± 0.09	–	0.30 ± 0.13	–	7.44 ± 0.09	not known
	13 Jun. 2010	21:45	22.44 ± 0.14	–	0.33 ± 0.18	–	7.20 ± 0.14	
(136204) 2003 WL7	15 Oct. 2009	00:38	20.70 ± 0.08	0.78 ± 0.08	0.45 ± 0.06	–	9.05 ± 0.08	0.05 ± 0.01[b]
			20.72 ± 0.05	...	...	...	9.07 ± 0.05	
	15 Oct. 2009	03:14	20.78 ± 0.06	0.67 ± 0.07	–	0.68 ± 0.06	9.13 ± 0.06	
	16 Oct. 2009	04:01	20.82 ± 0.05	0.68 ± 0.07	–	0.65 ± 0.05	9.17 ± 0.05	
			20.73 ± 0.05	...	...	...	9.08 ± 0.05	
(145452) 2005 RN43	11 Jun. 2010	03:15	20.13 ± 0.03	0.95 ± 0.05	0.60 ± 0.04	1.08 ± 0.05	4.05 ± 0.03	0.04 ± 0.01[b]
			20.16 ± 0.03	...	...	...	4.08 ± 0.03	
	12 Jun. 2010	03:55	20.16 ± 0.03	0.95 ± 0.04	0.59 ± 0.04	1.10 ± 0.05	4.08 ± 0.03	
			20.17 ± 0.03	...	...	...	4.09 ± 0.03	
	13 Jun. 2010	02:19	20.18 ± 0.04	0.93 ± 0.06	0.56 ± 0.05	1.02 ± 0.05	4.10 ± 0.04	
			20.19 ± 0.04	...	...	...	4.11 ± 0.04	
	14 Jun. 2010	03:52	20.15 ± 0.03	0.93 ± 0.04	0.61 ± 0.04	1.10 ± 0.04	4.07 ± 0.03	
			20.16 ± 0.03	...	...	...	4.08 ± 0.03	
(145480) 2005 TB190	26 Jun. 2009	03:03	21.51 ± 0.07	–	0.57 ± 0.10	1.28 ± 0.10	4.86 ± 0.07	0.12 ± 0.01[c]
(145486) 2005 UJ438	16 Oct. 2009	02:19	20.97 ± 0.04	0.84 ± 0.05	0.66 ± 0.05	1.17 ± 0.05	11.82 ± 0.04	0.13 ± 0.01[b]
			21.02 ± 0.04	...	...	...	11.87 ± 0.04	
(174567) 2003 MW12	22 Jun. 2009	23:45	20.43 ± 0.04	0.90 ± 0.04	0.56 ± 0.07	1.05 ± 0.05	3.67 ± 0.04	0.06 ± 0.01[b]
			20.44 ± 0.02	...	...	...	3.68 ± 0.02	
	23 Jun. 2009	23:00	20.45 ± 0.03	0.90 ± 0.04	0.55 ± 0.04	1.07 ± 0.05	3.69 ± 0.03	
			20.45 ± 0.03	...	...	...	3.69 ± 0.03	
	24 Jun. 2009	00:24	20.43 ± 0.03	0.85 ± 0.07	0.53 ± 0.05	1.09 ± 0.07	3.67 ± 0.03	
			20.41 ± 0.04	...	...	...	3.65 ± 0.04	
(248835) 2006 SX368	24 Jun. 2009	04:20	20.67 ± 0.04	–	0.48 ± 0.06	0.92 ± 0.05	9.94 ± 0.04	not known
	25 Jun. 2009	01:32	20.64 ± 0.04	0.76 ± 0.06	0.51 ± 0.06	1.00 ± 0.06	9.91 ± 0.04	
			20.63 ± 0.03	...	...	...	9.90 ± 0.03	
	25 Jun. 2009	03:49	20.73 ± 0.03	0.80 ± 0.05	0.47 ± 0.04	0.95 ± 0.04	10.00 ± 0.03	
			20.73 ± 0.03	...	...	...	10.00 ± 0.03	
(281371) 2008 FC76	13 Jun. 2010	03:15	20.41 ± 0.02	0.99 ± 0.04	0.70 ± 0.04	1.33 ± 0.04	10.04 ± 0.02	not known
			20.36 ± 0.02	...	...	...	9.99 ± 0.02	
	14 Jun. 2010	02:28	20.38 ± 0.02	1.01 ± 0.03	0.64 ± 0.03	1.32 ± 0.03	10.01 ± 0.02	
			20.38 ± 0.02	...	...	...	10.01 ± 0.02	

Notes. [a] From Dotto et al. (2008). [b] From Thirouin et al. (2010). [c] From Thirouin et al. (2012).

Table 2. continued.

Object	Date	UT_{start}	V	$B-V$	$V-R$	$V-I$	$H(\alpha)$	Light curve ampl.
(303775) 2005 QU182	14 Oct. 2009	23:28	20.71 ± 0.03	0.94 ± 0.06	0.64 ± 0.05	–	3.92 ± 0.03	not known
			20.71 ± 0.03	...	...	...	3.92 ± 0.03	
	15 Oct. 2009	22:20	20.83 ± 0.03	0.82 ± 0.05	0.61 ± 0.05	–	4.04 ± 0.03	
			20.82 ± 0.03	...	...	...	4.03 ± 0.03	
	16 Oct. 2009	01:00	20.72 ± 0.03	0.88 ± 0.05	0.53 ± 0.05	–	3.93 ± 0.03	
			20.74 ± 0.03	...	...	...	3.95 ± 0.03	
(307251) 2002 KW14	25 Jun. 2009	00:20	22.06 ± 0.03	–	0.74 ± 0.05	–	6.02 ± 0.03	0.21 ± 0.03[c]
	25 Jun. 2009	23:33	22.00 ± 0.04	–	0.64 ± 0.06	1.73 ± 0.07	5.96 ± 0.04	
(307982) 2004 PG115	23 Jun. 2009	01:36	21.11 ± 0.05	1.03 ± 0.08	0.58 ± 0.08	1.22 ± 0.09	5.50 ± 0.05	not known
			21.13 ± 0.04	...	...	...	5.52 ± 0.04	
	23 Jun. 2009	04:16	21.06 ± 0.05	0.96 ± 0.10	0.61 ± 0.07	1.24 ± 0.08	5.45 ± 0.05	
	24 Jun. 2009	02:11	21.07 ± 0.04	0.99 ± 0.06	0.59 ± 0.06	1.22 ± 0.15	5.46 ± 0.04	
			21.11 ± 0.04	...	...	...	5.50 ± 0.04	
	14 Oct. 2009	21:46	21.15 ± 0.04	0.92 ± 0.10	0.70 ± 0.06	–	5.52 ± 0.04	
			21.17 ± 0.04	...	...	...	5.54 ± 0.04	
	15 Oct. 2009	19:43	21.16 ± 0.03	0.93 ± 0.05	0.74 ± 0.05	–	5.53 ± 0.03	
			21.15 ± 0.04	...	...	...	5.52 ± 0.04	
	15 Oct. 2009	21:17	21.09 ± 0.04	0.97 ± 0.05	0.71 ± 0.05	–	5.46 ± 0.04	
			21.05 ± 0.04	...	...	...	5.42 ± 0.04	
2003 FE128	24 Jun. 2009	21:53	22.41 ± 0.04	–	0.69 ± 0.09	1.27 ± 0.08	6.90 ± 0.04	not known
			22.48 ± 0.04	...	...	...	6.97 ± 0.04	
	25 Jun. 2009	21:49	22.41 ± 0.04	–	0.69 ± 0.06	–	6.90 ± 0.04	
			22.44 ± 0.04	...	...	...	6.93 ± 0.04	
	12 Jun. 2010	23:04	22.60 ± 0.09	–	0.77 ± 0.11	1.39 ± 0.11	7.10 ± 0.09	
			22.57 ± 0.09	...	...	...	7.07 ± 0.09	
	13 Jun. 2010	23:32	22.48 ± 0.06	–	0.66 ± 0.09	–	6.98 ± 0.06	
2003 GH55	10 Jun. 2010	23:29	22.62 ± 0.05	–	0.72 ± 0.07	1.51 ± 0.12	6.55 ± 0.05	not known
			22.59 ± 0.05	...		..	6.52 ± 0.05	
	12 Jun. 2010	00:05	22.59 ± 0.05	–	0.65 ± 0.08	1.58 ± 0.12	6.52 ± 0.05	
2004 NT33	23 Jun. 2009	00:59	20.65 ± 0.02	0.64 ± 0.05	0.41 ± 0.04	0.83 ± 0.07	4.87 ± 0.02	0.04 ± 0.01[c]
			20.65 ± 0.04	...	...	...	4.87 ± 0.04	
	23 Jun. 2009	02:25	20.68 ± 0.04	0.65 ± 0.06	0.39 ± 0.05	0.83 ± 0.07	4.90 ± 0.04	
			20.67 ± 0.04	...	...	...	4.89 ± 0.04	
	24 Jun. 2009	01:34	20.67 ± 0.06	0.63 ± 0.09	0.41 ± 0.07	0.75 ± 0.07	4.89 ± 0.06	
			20.71 ± 0.05	...	...	...	4.93 ± 0.05	
2007 OC10	25 Jun. 2009	02:37	21.04 ± 0.04	0.87 ± 0.09	0.54 ± 0.07	1.02 ± 0.06	5.59 ± 0.04	not known
			21.09 ± 0.03	...	...	...	5.64 ± 0.03	
	26 Jun. 2009	01:19	21.03 ± 0.04	0.90 ± 0.08	0.55 ± 0.07	1.04 ± 0.08	5.58 ± 0.04	
			21.04 ± 0.04	...	...	...	5.59 ± 0.04	
		03:49	21.04 ± 0.04	0.86 ± 0.07	0.57 ± 0.07	1.01 ± 0.09	5.59 ± 0.04	
			20.98 ± 0.05	...	...	...	5.53 ± 0.05	

derived absolute magnitudes). These are the mean values of the most accurate measurements of phase coefficients for TNOs and Centaurs (Belskaya et al. 2008; Rabinowitz et al. 2008; Thirouin et al. 2012; this work). The obtained values from each $H(\alpha)$ measurement were then averaged to produce a final value of H_V for each object.

To consider the uncertainty associated with the light curve amplitude, we quadratically added 88% of the half amplitude (1σ, i.e. ~68%, of the values of a sinusoid are within this range) to the final uncertainty on H_V. For objects whose light curve amplitude is not available in the literature, we assumed a peak-to-peak amplitude of 0.2 mag (from the analysis of 74 objects, Duffard et al. 2009 found that 70% of TNOs and Centaurs have light curve amplitudes within this limit), hence we quadratically added 0.09 mag to the uncertainty on H_V.

The results of the above analysis are summarized in Table 3, which shows the obtained values of H_V for each of our targets. These absolute magnitudes are intended as values that can be readily used in combination with thermal measurements to derive the size and albedo of the investigated targets. Some of the measurements presented in this paper have already been combined with *Herschel* data by Vilenius et al. (2012) and Santos-Sanz et al. (2012).

3.2. Taxonomy

Based on their color indices, we derived the taxonomic classification of our targets via the G-mode method presented in Fulchignoni et al. (2000), using the taxonomy for TNOs and Centaurs introduced by Barucci et al. (2005) and extended by Fulchignoni et al. (2008). This taxonomy identifies four classes that reasonably indicate different composition and/or evolutional history, with increasingly red colors: *BB* (neutral colors with respect to the Sun), *BR*, *IR*, *RR* (red, very red colors). We classified each object whenever its colors were within 3σ of the class' average values. If more than one class was within 3σ, we assigned a multiple designation to the object, with taxonomic

Table 3. Computed absolute magnitudes.

Object	N	α (deg)	β (mag/deg)	H_V (mag)	References (other than this work)
(65489) Ceto [2003 FX128]	14	0.8–1.7	0.10 ± 0.06	6.58 ± 0.10	Tegler et al. (2003), Grundy et al. (2007), Ofek (2012)
(120061) 2003 CO1	7	1.8–5.1	0.09 ± 0.01	9.07 ± 0.05	Tegler et al. (2003), Perna et al. (2010)
(120178) 2003 OP32	6	0.8–1.3	0.05 ± 0.08	3.99 ± 0.11	Perna et al. (2010)
(120216) 2004 EW95	4	1.7	0.12 ± 0.06*	6.39 ± 0.15	–
(120347) Salacia [2004 SB60]	6	0.8–1.3	0.04 ± 0.06	4.26 ± 0.06	Benecchi et al. (2009)
(133067) 2003 FB128	2	1.1	0.12 ± 0.06*	7.09 ± 0.20	–
(136204) 2003 WL7	5	2.7–2.8	0.09 ± 0.04*	8.75 ± 0.16	–
(145452) 2005 RN43	18	0.4–1.4	0.18 ± 0.03	3.72 ± 0.05	DeMeo et al. (2009), Ofek (2012)
(145480) 2005 TB190	1	1.2	0.12 ± 0.06*	4.62 ± 0.15	–
(145486) 2005 UJ438	2	6.8	0.09 ± 0.04*	11.14 ± 0.32	–
(174567) 2003 MW12	6	0.6	0.12 ± 0.06*	3.51 ± 0.06	–
(248835) 2006 SX368	5	4.6	0.09 ± 0.04*	9.44 ± 0.25	–
(281371) 2008 FC76	5	3.5–5.3	0.09 ± 0.02	9.43 ± 0.13	Perna et al. (2010)
(303775) 2005 QU182	6	0.4	0.12 ± 0.06*	3.82 ± 0.12	–
(307251) 2002 KW14	2	0.8	0.12 ± 0.06*	5.79 ± 0.13	–
(307982) 2004 PG115	11	1.2–1.4	0.12 ± 0.06*	5.23 ± 0.15	–
2003 FE128	7	1.0–1.3	0.12 ± 0.06*	6.74 ± 0.18	–
2003 GH55	3	0.9	0.12 ± 0.06*	6.32 ± 0.13	–
2004 NT33	6	1.2–1.3	0.12 ± 0.06*	4.64 ± 0.09	–
2007 OC10	6	1.1	0.12 ± 0.06*	5.36 ± 0.13	–

Notes. N is the number of data points ($H(\alpha)$) combined from this work and literature. α is the phase-angle range covered by the available observations. β is the linear phase coefficient, whether fitted or assumed a priori [(*)]. The SDSS (g, r) magnitudes reported by Ofek (2012) have been converted to V magnitudes following Lupton (2005), see http://www.sdss.org/dr5/algorithms/sdssUBVRITransform.html. The reported absolute magnitudes H_V consider an assumed opposition surge of 0.1 mag, and light curve uncertainty. See text for more details.

Table 4. Taxonomic classification.

Object	Dyn. class	Taxonomy	Prev. tax.
(65489) Ceto [2003 FX128]	scattered	*IR*, *BR*	–
(120061) 2003 CO1	centaur	*BR*	*BR*[a]
(120178) 2003 OP32	classical	*BB*	*BB*[b]
(120216) 2004 EW95	resonant (3:2)	*BB*	–
(120347) Salacia [2004 SB60]	classical	*BR*	–
(133067) 2003 FB128	resonant (3:2)	*BB*, *BR**	–
(136204) 2003 WL7	centaur	*BB*	–
(145452) 2005 RN43[c]	classical	*IR*, *RR*	*RR*, *IR*[b]
(145480) 2005 TB190	detached	*IR*, *RR**	–
(145486) 2005 UJ438	centaur	*RR*, *IR*	–
(174567) 2003 MW12	classical	*IR*	*IR*, *BR*, *RR*[a]
(248835) 2006 SX368	centaur	*BR*	–
(281371) 2008 FC76	centaur	*RR*	*RR*[a]
(303775) 2005 QU182	scattered	*IR*, *RR**	–
(307251) 2002 KW14	classical	*RR**	–
(307982) 2004 PG115	scattered	*RR*, *IR*	–
2003 FE128	resonant (2:1)	*RR**	–
2003 GH55	classical	*RR**	–
2004 NT33	classical	*BB*, *BR*	–
2007 OC10	scattered	*IR*, *BR*	–

Notes. [(*)] Tentative classification based on two color indices only, for all objects but 2003 FB128. In this latter case, taxonomic classification is not possible, but the only available color index would be compatible with *BB*, *BR* taxa. [(a)] From Perna et al. (2010). [(b)] From Barucci et al. (2011). [(c)] For the statistical analysis presented in Sect. 3.2, we considered this object as an *RR*-type: the classification by Barucci et al. (2011) is based on near-infrared colors, where it is easier to distinguish between different taxa with respect to visible colors.

classes ordered by ascending deviation of the object colors from the class averages. Though we considered the classification reliable only when three color indices were available (which is the case for 14 out of our 20 targets), we also provide a "tentative" classification for five more objects, based on two color indices only. For (133067) 2003 FB128, with a single color index, the G-mode is not applicable: we can only state that the $V - R$ color would be compatible with a *BB*, *BR* classification. The obtained taxonomic designations are reported in Table 4, along with previous taxonomic classifications of the targets whenever available.

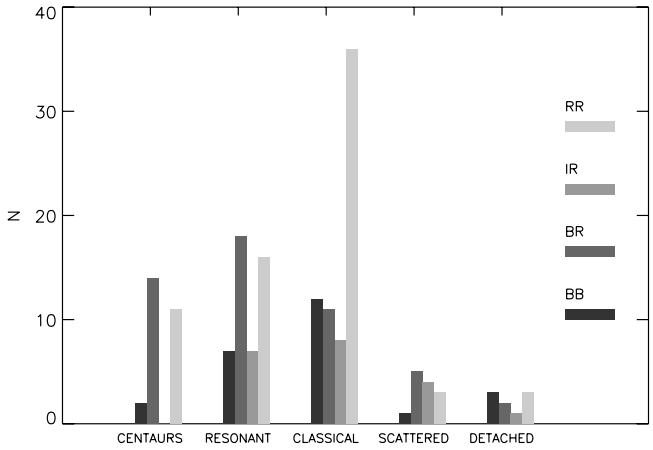

Fig. 1. Distribution of the taxa within each dynamical class.

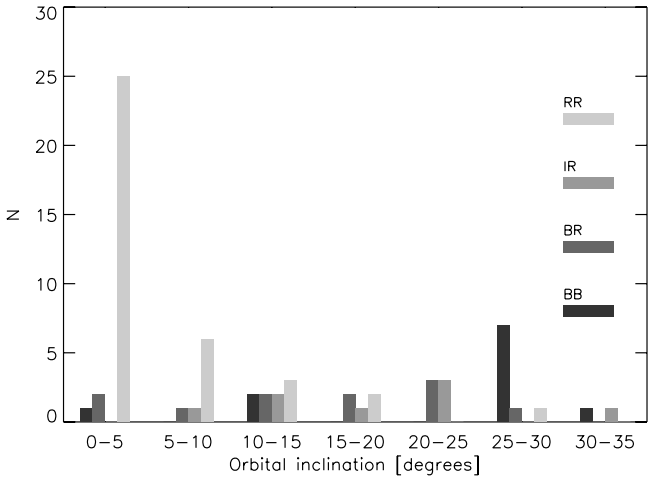

Fig. 2. Distribution of the taxa with respect to the orbital inclination of classical TNOs. A 5° binning is adopted.

Only the "robust" taxonomy that we obtained for 14 objects is included in the following analysis.

In this work we taxonomically classified nine objects for the first time. We combined our results with the literature (Fulchignoni et al. 2008; DeMeo et al. 2009; Perna et al. 2010; Barucci et al. 2011) for a total of 164 objects classified thus far, checking for correlations between colors, absolute magnitudes, and dynamical properties of TNOs and Centaurs.

From the distribution of the taxa within the different dynamical classes (Fig. 1), we confirm that *RR* objects dominate (36 out of 67 objects) the classical TNOs (e.g., Fulchignoni et al. 2008). The apparent color bimodality – with a "blue/gray" population and a "red" population – of Centaurs (e.g., Peixinho et al. 2003) is also confirmed. In particular, Centaurs completely lack *IR* types. Considering that Centaurs probably mostly come from other TNO dynamical classes (e.g., Levison & Duncan 1997), and also that the *IR* class is the only whose members do not present water ice features in their spectra (Barucci et al. 2011), this could suggest an evolutionary scenario for the color dichotomy of Centaurs. This agrees with the results of the numerical simulations by Melita & Licandro (2012), who have found considerable differences in the time spent in the past by "gray", "red", and active Centaurs (with the latter having colors similar to the gray group) below typical heliocentric distances: the red group penetrates less far into the inner solar system than gray and active objects, and the authors hence suggested that the observed color dichotomy is the result of the different thermal processing suffered on the surfaces of red and gray bodies. Noteworthy, all three active Centaurs whose taxonomical classification is available in the literature have blue/gray colors (Chiron is a *BB*-type, Echeclus and 2006 SX368 are *BR*-types; from Fulchignoni et al. 2008, and this work).

Figure 2 reports the distribution of the taxa with respect to the orbital inclination of the classical TNOs: inclinations of *RR*-types are low, in agreement with the previous finding of a red dynamically "cold" population. *BB*-types are instead concentrated at high inclinations, confirming the suggested association of these objects with the "hot" population (e.g., Doressoundiram et al. 2002). Our results agree with the finding, based on visible colors, that the color break occurs at ∼12° (Peixinho et al. 2008; Fornasier et al. 2009).

We found no other correlation between the taxonomical classification and the orbital parameters of objects belonging to the different dynamical groups, or with their absolute magnitude. This could support the hypothesis of Brown et al. (2011), who suggested that the currently observable surface compositions are correlated with the heliocentric distances where the different objects have formed, and that a strong mixing occurred after the TNO formation. In this scenario, the population of the red cold classicals would represent the only exception, with objects that formed in situ. Nevertheless, it is still difficult to draw a safe scenario for the formation and evolution of TNOs and Centaurs, because of the lack of fundamental data such as reliable albedo, size, and mass distributions. Results from the *Herschel* observations of TNOs will help in this sense.

3.3. Coma search in Centaurs

The Centaurs have orbital lifetimes shorter than 10^7 years (Holman & Wisdom 1993) and are considered transition objects between the TNOs and the Jupiter-family comets and other small-body populations closer to the Sun (e.g., Levison & Duncan 1997). About 10% of the total population of Centaurs has been found to show a comet-like activity at heliocentric distances up to about 13 AU (for a recent review about the active Centaurs, see Jewitt 2009). Many of these bodies had dust-loss rates comparable to or even higher than several active comets at much smaller heliocentric distance: for example, Mazzotta Epifani et al. (2011) found a dust production rate of 133 kg s^{-1} for P/2004 A1 (LONEOS) when it was at 6.5 AU from the Sun. The activity among Centaurs is part of a wider debate on the activity of small bodies at distances greater than 5–6 AU from the Sun, where classical water ice direct sublimation cannot work and other mechanisms, such as sublimation or release of very volatile ices (e.g., CO or CO2), have to be invoked (Meech & Svoren 2004).

Among the objects we studied at TNG are five Centaurs, observed at heliocentric distances between 8.3 and 15 AU. Hence we searched for an even faint coma around the "nuclei" in our images taken with the *R*-band filter (centered at $\lambda = 644$ nm, with a FWHM of 148 nm), which is the best indicated to verify the presence of a dust coma. No evidence of a coma emerged from point spread function (PSF) analysis for any of the five Centaurs. As an example, for Centaur 2006 SX368, Fig. 3 shows in black the mean (average of four profiles centered on the Centaur optocenter) object profile in the *R* image acquired on June 24, 2009 (exposure time of 450 s), compared with the mean stellar profile (in red), which was computed from several stars in photometric standard fields observed just after 2006 SX368.

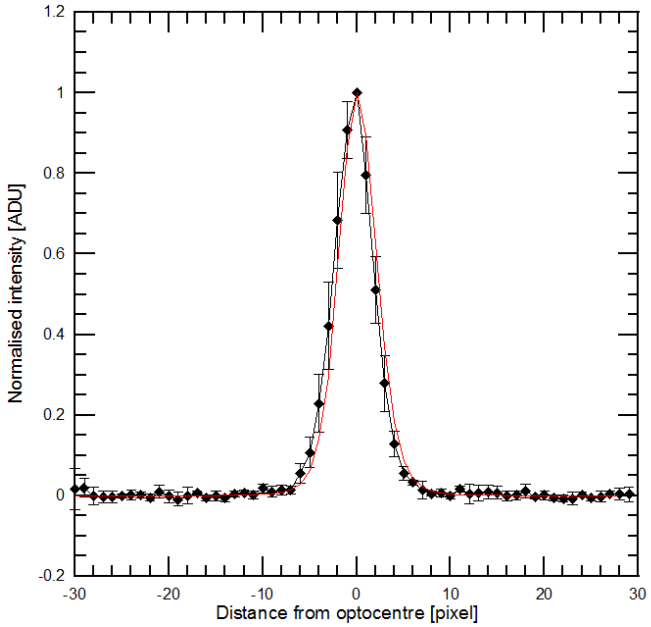

Fig. 3. Comparison between the mean profile of Centaur 2006 SX368 (black: dots are the pixel values with associated error bars), observed with the *R* filter on June 24, 2009, and the mean stellar profile (red).

To secure our result, we also computed the mean PSF profile from stars in the same image of the object, extracted perpendicularly to the apparent motion of the Centaur, and obtained similar results.

However, Centaur 2006 SX368 has been described as active by Jewitt (2009): he measured a dust mass-loss rate of 29 kg s^{-1} when the object was at 12.4 AU from the Sun (on September 19, 2007, with some assumptions on albedo, dust grain velocity, etc. – see below). If we assume that a still-unresolved coma is present in our images around the nucleus of 2006 SX368, we can at least estimate the dust production $Q_{\rm dust}$ by means of the "photometric model" introduced by Jewitt (2009). We have already applied this model to the active Centaur P/2004 A1 (LONEOS), with some considerations on the critical questions of the dust grain size distribution and of the radial outflow speed of dust grains from the nucleus (see Mazzotta Epifani et al. 2011, for more details). Here we recall only that the dust velocity is strictly dependant on dust size, dust-gas coupling efficiency, gas production rate, and many other factors (see, e.g., Newburn & Spinrad 1985, for a detailed description of the theory).

From the *V*-band albedo of 2006 SX368, $p_V = 0.055$ (Müller et al. 2010), and its mean $V - R$ color (Table 2), we derived the *R*-band albedo $p_R = 0.062$ to be used in the following expression to compute the total cross-section $C_{\rm d}$ of the coma dust particles in a coma annulus:

$$p_R \Phi(\alpha) C_{\rm d} = 2.25 \times 10^{22} \pi r^2 \Delta^2 10^{-0.4(m_{\rm d} - m_{\rm S})}, \quad (2)$$

where r, Δ and α are as in Eq. (1), $\Phi(\alpha) = 10^{-0.4\alpha\beta}$ represents the phase darkening (we used $\beta = 0.09$ mag/deg), $m_{\rm d}$ is the apparent magnitude of the pure coma in an annulus between two apertures ($\phi_1 = 1.1$ arcsec and $\phi_2 = 2.2$ arcsec were adopted to minimize the effects of nucleus contribution and sky background), and $m_{\rm S}$ is the apparent magnitude of the Sun in the *R* filter.

The photometric model allows one to relate (see Jewitt 2009 for more details) $C_{\rm d}$ to the dust mass $M_{\rm d}$ by adopting a power-law dust size distribution, and then relate it to the dust production rate $Q_{\rm dust}$ by considering the time of residence $\tau(r)$ of dust grains in the (projected) annulus between ϕ_1 and ϕ_2 ($\tau(r)$ obviously depends on the dust outflow velocity). To consider realistic values for these quantities (see Mazzotta Epifani & Palumbo 2011 for exhaustive considerations on these choices), we decided to adopt a dust size distribution such that the mean dust grain size is 30 μm, and a dust velocity ranging from 1 to 20 m/s. This range yields lower and upper limits to the possible dust production rate of 2006 SX368, with $Q_{\rm dust}$ ranging from 1 to 31 kg/s.

The dust production rate derived from our observations in June 2009 confirms that the cometary activity of 2006 SX368, if actually present, is rather weak, and constant along the Centaur orbit: reanalyzing the observational data obtained from Jewitt (2009) in September 2007, adopting the same parameters as above, we find a similar $Q_{\rm dust}$ range of 1 to 26 kg/s.

4. Conclusions

We performed at the TNG telescope visible photometric observations of 20 TNOs and Centaurs, targets of the "TNOs are cool" key program at the *Herschel* Space Observatory.

For each of our targets, we derived the absolute magnitude H_V. Because a correct knowledge of the H_V value is fundamental when applying the radiometric technique to derive the size and the albedo of the investigated objects, we took all precautions to provide an accurate determination of H_V and its error for each of our targets. Hence our values are intended as readily usable inputs to be used in combination with the *Herschel* data. We recall that knowing the size and albedo for all ~130 *Herschel* targets will provide important information on the early evolution of the solar system, because the size distribution of these bodies is supposed to be almost unchanged from the accretion phases.

From the visible colors of our targets, we found hints of a heterogeneous surface for (65489) Ceto, and derived the taxonomic classification for 14 objects. Nine of them were classified for the first time, the results for the remaining five objects agree with the available literature. Additional objects have been tentatively classified based on incomplete datasets, but we did not consider them for the subsequent analysis. We combined our results with the literature and took into account the 164 objects that have been taxonomically classified thus far to analyze their distribution with respect to the dynamical properties of the objects. Our results seem to support the most recent findings about an evolutionary origin for the well-known color dichotomy of Centaurs (e.g., Melita & Licandro 2012), as well as the occurrence of a strong mixing of TNOs after their formation (e.g., Brown et al. 2011).

With a PSF analysis, we searched for an even faint coma around the five Centaurs in our sample, including (248835) 2006 SX368, which was previously described as active by Jewitt (2009). We found no evidence of coma. Assuming that a still-unresolved coma is present around the nucleus of 2006 SX368, we used the photometric model (Jewitt 2009) to derive an estimate of the dust production rate. We found that possible values for $Q_{\rm dust}$ range from 1 to 31 kg/s, in agreement with the results by Jewitt (2009). This confirms that the cometary activity of 2006 SX368, if actually present, is weak and constant along its orbit.

References

Barucci, M. A., Romon, J., Doressoundiram, A., & Tholen, D. J. 2000, AJ, 120, 496
Barucci, M. A., Belskaya, I. N., Fulchignoni, M., & Birlan, M. 2005, AJ, 130, 1291

Barucci, M. A., Boehnhardt, H., Cruikshank, D. P., & Morbidelli, A. 2008, in The Solar System Beyond Neptune (Tucson: Univ. of Arizona Press), 3
Barucci, M. A., Alvarez-Candal, A., Merlin, F., et al. 2011, Icarus, 214, 297
Belskaya, I. N., Levasseur-Regourd, A.-C., Shkuratov, Y. G., & Muinonen, K. 2008, in The Solar System Beyond Neptune, eds. M. A. Barucci, H. Boehnhardt, D. P. Cruikshank, & A. Morbidelli (Tucson: Univ. of Arizona Press), 115
Benecchi, S. D., Noll, K. S., Grundy, W. M., et al. 2009, Icarus, 200, 292
Bowell, E., Hapke, B., Domingue, D., et al. 1989, in Asteroids II, eds. R. P. Binzel, T. Gehrels, & M. S. Matthews (Tucson: Univ. of Arizona Press), 524
Brown, M. E., Schaller, E. L., & Fraser, W. C. 2011, ApJ, 739, L60
Davis, D., & Farinella, P. 1997, Icarus, 125, 50
DeMeo, F. E., Fornasier, S., Barucci, M. A., et al. 2009, A&A, 493, 283
Doressoundiram, A., Peixinho, N., de Bergh, C., et al. 2002, AJ, 124, 2279
Dotto, E., Perna, D., Barucci, M. A., et al. 2008, A&A, 490, 829
Duffard, R., Ortiz, J. L., Thirouin, A., et al. 2009, A&A, 505, 1283
Fornasier, S., Barucci, M. A., de Bergh, C., et al. 2009, A&A, 508, 457
Fulchignoni, M., Birlan, M., & Barucci, M. A. 2000, Icarus, 146, 20
Fulchignoni, M., Belskaya, I., Barucci, M. A., de Sanctis, M. C., & Doressoundiram, A. 2008, in The Solar System Beyond Neptune, eds. M. A. Barucci, H. Boehnhardt, D. P. Cruikshank, & A. Morbidelli (Tucson: Univ. of Arizona Press), 181
Gladman, B., Marsden, B. G., & VanLaerhoven, C. 2008, in The Solar System Beyond Neptune, eds. M. A. Barucci, H. Boehnhardt, D. P. Cruikshank, & A. Morbidelli (Tucson: Univ. of Arizona Press), 43
Grundy, W. M., Stansberry, J. A., Noll, K. S., et al. 2007, Icarus, 191, 286
Holman, M. J., & Wisdom, J. 1993, AJ, 105, 1987
Jewitt, D. 2009, AJ, 137, 4296
Landolt, A. U. 1992, AJ, 104, 340
Levison, H. F., & Duncan, M. J. 1997, Icarus, 127, 13
Mazzotta Epifani, E., & Palumbo, P. 2011, A&A, 525, A62
Mazzotta Epifani, E., Dall'Ora, M., Perna, D., Palumbo, P., & Colangeli, L. 2011, MNRAS, 415, 3097
Meech, K. J. & Svoren, J. 2004, in Comets II, eds. M. Festou, H. U. Keller, & H. A. Weaver (Tucson: Univ. of Arizona Press), 317
Melita, M. D., & Licandro, J. 2012, A&A, 539, A144
Müller, T. G., Lellouch, E., Böhnhardt, H., et al. 2009, EM&P, 105, 209
Müller, T. G., Lellouch, E., Stansberry, J., et al. 2010, A&A, 518, L146
Newburn, R. L., & Spinrad, H. 1985, AJ, 90, 2591
Ofek E. O. 2012, ApJ, 749, 10
Peixinho, N., Doressoundiram, A., Delsanti, A., et al. 2003, A&A, 410, L29
Peixinho, N., Lacerda, P., & Jewitt, D. 2008, AJ, 136, 1837
Perna, D., Barucci, M. A., Fornasier, S., et al. 2010, A&A, 510, A53
Rabinowitz, D. L., Schaefer, B. E., Schaefer, M., & Tourtellotte, S. W. 2008, AJ, 136, 1502
Santos-Sanz, P., Lellouch, E., Fornasier, S., et al. 2012, A&A, 541, A92
Stansberry, J., Grundy, W., Brown, M., et al. 2008, in The Solar System Beyond Neptune, eds. M. A. Barucci, H. Boehnhardt, D. P. Cruikshank, & A. Morbidelli (Tucson: Univ. of Arizona Press), 161
Tegler, S. C., Romanishin, W., & Consolmagno, G. J. 2003, ApJ, 599, L49
Thirouin, A., Ortiz, J. L., Duffard, R., et al. 2010, A&A, 522, A93
Thirouin, A., Ortiz, J. L., Campo Bagatin, A., et al. 2012, MNRAS, 424, 3156
Vilenius, E., Kiss, C., Mommert, M., et al. 2012, A&A, 541, A94